OXFORD CENTRE FOR COLLABORATIVE APPLIED MATHEMATICS

Report Number 09/35

A metabolite-sensitive, thermodynamically-constrained model of cardiac cross-bridge cycling: Implications for force development during ischemia

by

Kenneth Tran, Nicolas P. Smith, Denis S. Loiselle, Edmund J. Crampin

Oxford Centre for Collaborative Applied Mathematics
Mathematical Institute
24 - 29 St Giles'
Oxford
OX1 3LB
England

A metabolite-sensitive, thermodynamically-constrained model of cardiac cross-bridge cycling: Implications for force development during ischemia

Kenneth Tran
Auckland Bioengineering Institute
University of Auckland, New Zealand

Nicolas P. Smith
University Computing Laboratory
University of Oxford, UK

Denis S. Loiselle
Auckland Bioengineering Institute
and Department of Physiology
University of Auckland, New Zealand

Edmund J. Crampin[1]
Auckland Bioengineering Institute
and Department of Engineering Science
University of Auckland, New Zealand

[1]Corresponding author: email: e.crampin@auckland.ac.nz

Abstract

We present a metabolically regulated model of cardiac active force generation with which we investigate the effects of ischemia on maximum force production. Our model, based on the Rice et al. (2008) model of cross-bridge kinetics, reproduces many of the observed effects of MgATP, MgADP, Pi and H^+ on force development while still retaining the force/length/Ca^{2+} properties of the original model. We introduce three new parameters to account for the competitive binding of H^+ to the Ca^{2+} binding site on troponin C and the binding of MgADP within the cross-bridge cycle. These parameters along with the Pi and H^+ regulatory steps within the cross-bridge cycle were constrained using data from the literature and validated using a range of metabolic and sinusoidal length perturbation protocols. The placement of the MgADP binding step between two strongly-bound and force-generating states leads to the emergence of an unexpected effect on the force-MgADP curve, where the trend of the relationship (positive or negative) depends on the concentrations of the other metabolites and $[H^+]$. The model is used to investigate the sensitivity of maximum force production to changes in metabolite concentrations during the development of ischemia.

Key words: Cross bridge; Cardiac muscle; Metabolism; Mathematical model; Ischemia; Thermodynamics

Introduction

In order for the heart to fulfil its function as a pump, its musculature must cyclically develop force, shorten and relax. This cycle is achieved by the expenditure of metabolic energy via pathways the end-products of which are inhibitory to the cycle. Such inhibition becomes particularly crucial during periods of hypoxia or ischemia when the reduction in supply of ATP from mitochondrial oxidative phosphorylation, and the attendant accumulation of inorganic phosphate (Pi), ADP and protons may interfere with the cyclic interactions between actin monomers and myosin heads protruding from the thick filaments (1).

Our aim is to develop a thermodynamically-consistent and metabolite-sensitive model of cardiac cross-bridge cycling in order to explore the influence of these metabolites on force production under physiological and ischemic conditions. There are a number of criteria that such a model must meet. The cycling action of cross-bridges is driven by the free energy released from the hydrolysis of ATP into ADP and Pi (free energy transduction). Firstly, therefore, the model must incorporate a free energy-transducing thermodynamic cycle, with pathways that allow it to be driven in both the forward and backward directions (2). This excludes 'fading memory' models which do not explicitly represent the cross-bridge cycle (3, 4). Secondly, the model must be thermodynamically consistent as defined by Hill (5) where a constraint is introduced to relate the rate constants of the model to the free energy of ATP hydrolysis. Thirdly, the model must explicitly incorporate the regulatory effects of MgATP and its hydrolysis products, MgADP, Pi and H^+. 'Sliding filament' models, derived from the seminal work of Huxley (6), are based on strain-dependent distributions of cross-bridge populations, and have been extended to include metabolite interactions (7). However, the explicit representation of a spatial dimension (cross-bridge strain) requires the solution of partial differential equations which renders them computationally expensive and not ideal for integrating into cell or tissue models. More recently, 'mean field' models have been proposed which ignore the microscopic details of cross-bridge population distributions but, instead, ascribe the behaviour of the entire cross-bridge population to an *average* cross-bridge cycle, removing the need for partial differential equations.

In this study we extend the recent mean field model by Rice et al. (8) such that it conforms to the criteria listed above. The Rice et al. (8) model describes Ca^{2+} activation and cross-bridge cycling kinetics and can reproduce a range of myofilament behaviour including length- and temperature-dependent effects. This model provides a foundation onto which a biochemi-

cal scheme of ATP hydrolysis is integrated to develop a thermodynamically-consistent and metabolite-sensitive model of cross-bridge cycling kinetics (which we denote as the *Extended Model*). The Extended Model introduces three new parameters which are fitted using cardiac data from the literature and validated against a range of metabolic and sinusoidal length change protocols. The model is then used to investigate the effects of changing metabolite concentrations, observed after the onset of ischemia, on the development of active force.

Methods

A schematic of the 4-state model by Rice et al. (8) is shown in Fig. 1A. Rice et al. parameterised their model for rat cardiac tissue, and include a parameter $xbmod_{species}$ (which multiplies all rate constants) to adjust to different species. Consistent with our previous studies (9–11), we develop a model parameterised for guinea pig myocardium, setting $xbmod_{species} = 0.2$, effectively slowing the kinetics by five-fold from rat, following the findings of Palmer and Kentish (12). We parameterise and validate against guinea pig data where possible.

The original model implicitly assumes that cross-bridge cycling is irreversible by omitting a reverse step between states P_{XB} and $XBpostR$. In order to account for the full (reversible) thermodynamic cycle we add a reverse transition step, f_{xbT} (Fig. 1B), to allow transitions from state P back to state $XBpostR$, representing the release of MgATP as the myosin head transitions from a weakly attached state back to a strongly attached state. The value of f_{xbT} is determined by the thermodynamic constraint which links the rate constants in the cycle to the hydrolysis of MgATP (5):

$$\frac{\prod \alpha_i^+}{\prod \alpha_i^-} = e^{\frac{-\Delta G_{ATP}}{RT}} \tag{1}$$

where α_i^+ and α_i^- are the *pseudo first order* forward and backward rate constants for state i and

$$\Delta G_{ATP} = \Delta G^0_{ATP} + RT \ln \frac{[\mathrm{MgADP}][\mathrm{Pi}][\mathrm{H}^+]}{[\mathrm{MgATP}]} \tag{2}$$

where ΔG^0_{ATP} is the standard free energy of MgATP hydrolysis and H^+ is the proton released during ATP hydrolysis, which we label the 'metabolic proton'. The equation for f_{xbT} is given in the Appendix.

Metabolite dependencies are incorporated into the transition rates between steps of the cycle using mass action kinetics. We will assume that normal physiological metabolic conditions are given by MgATP = 5 mM, MgADP = 36 μM, Pi = 2 mM, pH = 7.15, and that the parameters and outputs from Rice et al. (8) correspond to these conditions.

MgATP

The binding of MgATP in striated muscle detaches the cross-bridge from the strongly-bound state after execution of the power stroke (13–16). Measurements of isometric force have shown a descending trend with increasing concentrations of MgATP, consistent with the dissociation of strongly-bound cross-bridges (17, 18). In the Extended Model (Fig. 1B), the MgATP binding step is therefore placed in the transition from state XB_{PostR} to state P_{XB} (g_{xbT}) during which the strongly-bound cross-bridge becomes detached. It is also assumed that hydrolysis of ATP occurs at this step. The Rice et al. (8) parameter for the transition, g_{xbT}, is adjusted to account for physiological MgATP concentrations using the formulation:

$$g'_{xbT} = \frac{g_{xbT}}{MgATP'} \tag{3}$$

where g'_{xbT} represents the true first order rate constant, $MgATP'$ is the physiological MgATP concentration and g_{xbT} is the pseudo-first order rate constant from the Rice et al. (8) model. Following mass-action kinetics, the MgATP-dependent transition rate from state XB_{PostR} to state P_{XB} is therefore given by:

$$g'_{xbT} \times [\text{MgATP}] \tag{4}$$

Under normal metabolic conditions, when [MgATP] = $MgATP'$, this gives $g'_{xbT} = g_{xbT}$. This formulation is applied to the other metabolite dependencies described below. The equation for this transition rate is not yet complete as g'_{xbT} is also modified by MgADP (see below).

Inorganic Phosphate

Biochemical and mechanical experiments in both skeletal (19, 20) and cardiac (21, 22) muscle have demonstrated that increasing [Pi] leads to a decrease in isometric force. Under isometric conditions, the sole force-producing state in the Rice et al. (8) model is XB_{PostR} while XB_{preR} remains as a strongly-bound state that can contribute to cross-bridge stiffness. The binding of Pi can therefore be placed at either h_{bT} or g_{appT} as either

will drive the cross-bridge cycle away from XB_{PostR} and decrease isometric force with increasing [Pi]. We find that placing the Pi binding step at g_{appT} produces a better quantitative fit to the data (see below). The adjustment of the original rate constant to account for [Pi] is given by:

$$g'_{appT} = \frac{g_{appT}}{Pi'} \tag{5}$$

where the parameters are defined equivalently to those in Eq. 3.

pH

Changes in pH have been shown to affect the force-Ca curve in two distinct ways. A decrease of pH leads to a decrease in the Ca^{2+} sensitivity as well as a decrease in the maximum force generated at saturating levels of Ca^{2+} (23, 24). To incorporate these effects, we include two distinct mechanisms of sensitivity to pH. We assume that the decrease in Ca^{2+} sensitivity with decreasing pH is due to the competitive binding of H^+ to the single Ca^{2+} binding site on troponin C (Fig. 1C) (25, 26), modelled as a rapid equilibrium reaction identically for both populations of troponin with dissociation constant k_{dHCa} and cooperativity m. This modifies the rate constant for the binding of Ca^{2+} to troponin C:

$$k'_{onT} = \frac{k^m_{dHCa} + H'^m}{k^m_{dHCa} + [H^+]^m} \times k_{onT} \tag{6}$$

where k'_{onT} is the new apparent rate constant for Ca^{2+} binding, k_{onT} is the original Ca^{2+} binding rate constant and H' is the reference proton concentration. The apparent rate constant for Ca^{2+} binding affects the transition rates responsible for activation of the cross-bridge cycle (k_{pnT} and k_{npT}). The two parameters that govern the mechanism of competitive H^+ binding, k_{dHCa} and m, are determined using data from the literature (see below).

The inclusion of competitive H^+ binding can account for the shift in Ca^{2+} sensitivity but cannot reproduce the change in maximum tension at saturating Ca^{2+} concentration. This effect can be incorporated by assigning one of the (reverse) rate constants in the cross-bridge cycle (Fig. 1A) to be associated with the release of the metabolic H^+ (a by-product of the ATP hydrolysis reaction, Eq. 2). The two positions at which this reaction could occur are h_{bT} and g_{appT} as both can lead to a decrease in force with an increase in H^+ concentration. We locate H^+ release at the reverse isomerization step, h_{bT} because this produces a drop in force of a magnitude that

is in better agreement with the data (see below). The adjustment of the rate constant to account for the physiological H^+ concentration is given by:

$$h'_{bT} = \frac{h_{bT}}{H'} \tag{7}$$

where the parameters are defined equivalently to those in Eq. 3. The H^+-dependent transition from XB_{PostR} to XB_{PreR} is therefore given by:

$$h'_{bT} \times [H^+] \tag{8}$$

The equation for this transition rate is also not yet complete as h'_{bT} is also modified by MgADP (see below).

MgADP

Mechanical measurements have shown that MgADP binds to *attached* cross-bridges (27–30) which remain attached after the binding event (31). Increasing MgADP concentrations also leads to an increase in steady-state isometric force development in both skeletal (17, 32) and cardiac (21, 33) muscle preparations. The only transition between strongly-bound states in the four-state Rice et al. (8) model where the MgADP binding event could be placed is from $XBpostR$ to $XBpreR$. This, however, leads to a *decrease* in isometric force development because $XBpreR$ is a lower-force state than $XBpostR$. The four-state model therefore contains an insufficient number of states to represent the binding of MgADP and hence we expand state $XBPostR$ into two force-producing sub-states, $AM1$ and $AM2$ to create a five-state model (Fig. 1B), where we assume that the two sub-states contribute equally to total force and sum to produce the same force as state $XBpostR$, and MgADP is assumed to bind to state $AM1$. This five-state construction is equivalent to the four-state model when binding and unbinding of MgADP is rapid (states $AM1$ and $AM2$ are in rapid equilibrium). We model the MgADP binding step with a single parameter representing the MgADP dissociation constant, k_{dADP}. This modifies the rates of transitions *leaving* state XB_{PostR} *i.e.,* g'_{xbT} and h'_{bT} by:

$$\frac{k_{dADP} + MgADP'}{k_{dADP} + [\mathrm{MgADP}]}$$

and

$$\left(\frac{k_{dADP} + MgADP'}{MgADP'}\right) \times \left(\frac{[\mathrm{MgADP}]}{k_{dADP} + [\mathrm{MgADP}]}\right)$$

respectively, where $MgADP'$ is the normal physiological MgADP concentration and the dissociation constant k_{dADP} is constrained by fitting the model to isometric force data (see below). Incorporating Eq. 4, the complete MgATP and MgADP-dependent transition from XB_{PostR} to P_{XB} is given by:

$$[\text{MgATP}] \times g'_{xbT} \times \left(\frac{k_{dADP} + MgADP'}{k_{dADP} + [\text{MgADP}]} \right) \tag{9}$$

By incorporating Eq. 8, the complete H^+ and MgADP-dependent transition from XB_{PostR} to XB_{PreR} is determined:

$$[H^+] \times h'_{bT} \times \left(\frac{k_{dADP} + MgADP'}{MgADP'} \times \frac{[\text{MgADP}]}{k_{dADP} + [\text{MgADP}]} \right) \tag{10}$$

A full description of the model formulation and equations that have been modified from Rice et al. (8) is given in the accompanying Supporting Material.

Parameter estimation and model selection

Previous studies have suggested that placement of the Pi-binding step at either g_{appT} or h_{bT} provides plausible explanations for the isometric force-Pi data (19, 20, 34). We found that the Extended Model best fits the data when the Pi binding step is placed at g_{appT} (Fig. 2A). There is also evidence demonstrating a decrease in stiffness with increased [Pi], which is consistent with the binding of Pi causing the dissociation of cross-bridge attachment (3, 35). This leaves the binding location of the metabolic H^+ along with the three new parameters, k_{dADP}, k_{dHCa} and m, to be determined.

Experiments in cardiac muscle preparations have measured an increase in isometric force of approximately 10-15% when [MgADP] is increased from zero to saturating concentrations in the millimolar range (21). We constrain the MgADP dissociation constant, k_{dADP}, to give a 13% increase in isometric force when [MgADP] is increased from 0 to 3 mM (21). This produces a k_{dADP} value of 4 μM which compares well with those measured by Johnson and Adams (36) (14 μm at 23 °C and 5 μm at 15 °C) and Kardami et al. (37) (8 μm at 5 °C) which were obtained from bovine cardiac preparations using independent assaying methodologies.

To determine the parameters governing the competitive binding of H^+ to the Ca^{2+} binding sites on troponin C, we use the guinea pig force-Ca data of Orchard and Kentish (24). For reasons considered in the Discussion, the slopes of the force-Ca data are relatively flat ($n = 2$) when compared to the curves produced by the Rice et al. (8) model ($n = 7$). Therefore we fit

the *relative* change in Ca^{2+} sensitivity (Ca_{50}) brought about by changes in H^+ concentration. Fig. 2B shows the result of fitting the Extended Model to the normalised data from Orchard and Kentish (24). The Ca_{50} values for the data set have been normalised to the Ca_{50} at pH = 7. The best fit to the data is obtained at $m = 1$ and $k_{dHCa} = 2 \times 10^{-5}$ mM. For increasing values of m, the curve becomes more concave and does not fit the data as well. The value of 1 for the cooperativity constant, m, can be interpreted as the binding of a single H^+ to the Ca^{2+} binding site and, in this model, is favoured over the binding of two or more H^+.

Fig. 2C shows model simulations when the metabolic H^+ is released at either g_{appT} or h_{bT} (Fig. 1B). Both simulations are qualitatively consistent with the data inasmuch as a decrease of pH leads to a decrease in maximum steady-state force. However, quantitatively, the placement of the H^+ release step at h_{bT} produces better agreement with the data from Orchard and Kentish (24) (guinea pig trabeculae) and Godt and Nosek (21) (rabbit papillary). Fig. 2D shows the overall effect of pH on the force-Ca curve, giving the expected decrease in Ca^{2+} sensitivity and maximum force with decreasing pH, comparable to experimental data from Orchard and Kentish (24) (shown in the Supporting Material—but exhibiting a much steeper slope because the experimental data of Orchard and Kentish (24) are from skinned preparations).

Results

Force redevelopment and MgATP

The Extended Model was used to predict the effect of varying MgATP concentration on the isometric force response and the rate of tension redevelopment after a sudden length change (Fig. 3A). An increase in MgATP concentration leads to a decrease in the normalised force as this favours the detachment of strongly-bound crossbridges (g'_{xbT}) thereby reducing the proportion of cross-bridges in the strongly-bound state. The model simulations show that the force-MgATP curve is sensitive to low levels of MgADP concentration, as decrease of MgADP represents a reduction in the competition for the strongly-bound state $AM1$ which results in a large drop in force with increasing MgATP. The data set from Ebus et al. (18) lies within the family of curves simulated by the model at low to physiological MgADP concentrations. Fig. 3B and C show the force redevelopment after the imposition of a sudden length change, which is assumed to detach almost all the strongly-bound cross-bridges thus reducing the developed force

to zero, at three different MgATP concentrations. Rapid detachment of cross-bridges is simulated (at time $t = 300$ ms) by decreasing 1000-fold the forward transition rates, f_{appT} and h_{fT}, and increasing 1000-fold the backward rate constants, g'_{appT} and h'_{bT}, for a period of 5 ms. Fig. 3B shows that the steady-state force increases with decreasing MgATP concentration, consistent with Fig. 3A, while Fig. 3C shows that the rate of tension redevelopment *decreases* with decreasing MgATP concentration. These predictions are consistent with the results of Ebus et al. (18) (Fig. 3D) who also demonstrated a decrease in rate of tension redevelopment with decreasing MgATP concentrations.

Sinusoidal length perturbations

Kawai et al. (3) used sinusoidal length perturbation over a range of frequencies to determine the complex stiffness of cardiac muscle at different MgATP and Pi concentrations (in ferret myocardium). We imposed a sinusoidal length change with an amplitude of 0.25% of L_0, the 'imposed sarcomere length' (2.28 μm) in the Extended Model, including both passive and active components of tension. Figure 4 shows the two components of complex stiffness, dynamic modulus (A) and phase shift (B), as a function of perturbation frequency at different Pi concentrations, compared with the experimental data from Kawai et al. (3). (Similar plots showing the comparison between model and data for dynamic modulus and phase shift at different MgATP concentrations can be found in the accompanying Supporting Material, and provide further validation of the dependence of cross-bridge cycling on MgATP.)

Our simulations reproduce, qualitatively and semi-quantitatively, features observed in the experimental data. Both demonstrate that with increasing frequency the dynamic modulus increases, whereas the phase shift increases towards a peak before decreasing. Dynamic modulus is a measure of muscle stiffness, which is directly proportional to force and is therefore a function of the fraction of cross-bridges in the strongly-bound state and their mean distortions. In the model, stiffness increases with frequency because the average distortion of the strongly-bound cross-bridges increases before they can detach.

The response to a change in [Pi] (and in [MgATP]; see Supporting Material) is very similar to the experimental observations. Stiffness *decreases* with *increasing* [Pi] (Fig. 4A) while the peaks of the phase shifts move to a lower frequency. Increasing [Pi] (or [MgATP]) leads to a decrease in stiffness at a given stimulation frequency as it favors detachment of cross-bridges (re-

ducing the proportion in the strongly-bound state, and hence stiffness). An increase in [Pi] favors detachment of cross-bridges (from XB_{PreR}) in the anti-clockwise direction, while an increase in [MgATP] favors detachment (from XB_{PostR}) in the clockwise direction.

Force development during ischemia: sensitivity analysis

A key motivation for our study was to investigate the effects of changing metabolite concentrations during ischemia on the development of active force. Befroy et al. (38) measured [PCr], [ATP] and pH, and developed pressure, during 20 minutes of zero-flow global ischemia in perfused guinea pig hearts. These data were used by Terkildsen et al. (10) to calculate the time courses for [ADP] (using the creatine kinase equilibrium constant) and [Pi] (assuming conservation of the total phosphate pool). These time courses are shown in the first column of Fig. 5 (rows **A** to **D**), with the corresponding isometric force at maximum Ca^{2+} activation ($[Ca^{2+}] = 200$ μM; row **E**). calculated from the model. The simulation shows force decreasing rapidly to approximately 10% of its pre-ischemic value after about 10 minutes, consistent with the pressure measurements from Befroy et al. (38) and others (1).

To investigate the relative effects of the metabolites and pH on the maximum force during ischemia, we performed a sensitivity analysis at times T = 0 (normoxic conditions), and T = 2.5, 5, and 10 min after the onset of ischemia. Each curve shows the change in maximum force (y-axis) as one metabolite is varied (x-axis) while the others are held at their respective values for that time point (shown as filled circles on the sensitivity curves). For example, row **B** shows the negative inotropic effect of increasing [Pi] on force when [MgATP], [Pi] and pH are kept constant, while row **C** shows an initially positive effect of [MgADP] on force, but a small but negative effect on force after a few minutes of ischemia. Row **E** shows the effect of calcium on force at each time point post-onset of ischemia, showing that the calcium level required to achieve the diminishing maximal force also increases during the progression of ischemia.

These results indicate that the maximum force is most sensitive to changes in [Pi] and pH (the curves for [Pi] and pH have steepest gradient over the physiological range). The initial rapid decrease in maximum force after the onset of ischemia is primarily caused by increasing [Pi] and decreasing pH. We note, however, that these effects are not additive due to the nonlinear dependencies among variables in the model. Force is not strongly sensitive to MgATP or MgADP. At T = 0, increasing [MgATP] leads to a decrease

in force whereas after T = 2.5 min, force becomes insensitive to [MgATP]. For [MgADP], at T = 0 force increases with increasing [MgADP], becoming almost insensitive at T = 2.5 min and starts to decrease after T = 5 min. These changes in the sensitivity to [MgATP] and [MgADP] over the time course of ischemia are due to the changing [Pi] and pH levels. The switch from increasing to decreasing sensitivity to [MgADP] is a consequence of the MgADP binding step occuring between two strongly-bound states. The shift to the right (higher Ca) in the force-Ca curve (Row **E**) demonstrates the reduction of sensitivity to Ca^{2+} during ischemia. This is brought about primarily by the increased inhibition of Ca^{2+} binding to troponin C due to falling pH (Fig. 2D).

Discussion

The position of the MgATP and MgADP binding steps within the cross-bridge cycle are well constrained by data from the literature. MgATP was assumed to bind at g_{xbT} because this transition detaches a strongly-bound cross-bridge, consistent with experimental observations (7, 18). Experimental observations have also shown that the cross-bridge head remains strongly attached after the MgADP binding event, and that increasing [MgADP] leads to an increase in isometric force (21, 31, 33), which lead us to introduce a new state into the original cross-bridge scheme from Rice et al. (8). The binding positions for Pi and the metabolic H^+ in the cross-bridge cycle are not as well characterised in the literature. Data indicate that an increase in the concentrations of either Pi or H^+ will lead to a decrease in isometric force (21–24). This qualitative behaviour can be satisfied by placing either of these binding events at g_{appT} or h_{bT} (Fig. 1), and we have determined a scheme that gives the best fit to experimental data (Figs. 2A and 2C). Pi binding at g_{appt} is further supported by the sinusoidal length perturbation simulations in Fig. 4, which reproduce the qualitative, and many of the quantitative, aspects of the experimental data. (MgATP binding is also further supported by these simulations—see Supporting Material.) These simulations demonstrate the 'recruitment' and 'distortional' stiffnesses identified by Campbell et al. (39) who analytically derived the frequency response of the Razumova et al. (40) model—a precursor to the Rice et al. (8) model. The distortional stiffness rises with increasing frequency because the cross-bridges are stretched further before they can detach while the recruitment stiffness is a function of the fractional occupancies of the strongly-bound cross-bridge states (XB_{PreR} and XB_{PostR}). Increasing either [MgATP] or

[Pi] leads to a decrease in the fractional occupancy of these strongly-bound states, resulting in a decrease in stiffness, as is observed in the experimental data of Kawai et al. (3).

Decreasing pH, as occurs during ischemia, has been shown to affect the force-Ca curves in two distinct ways, shifting the force-Ca curve to the right (reducing Ca^{2+} sensitivity) (23–26, 41), and decreasing the maximum force at saturating Ca^{2+} (23, 24). We have shown that competitive binding of H^+ for the Ca^{2+} binding site on troponin C can account for the pH-dependent shift in Ca_{50} and that the release of the ATP hydrolysis-derived proton directly affects kinetics of the cross-bridge cycle, leading to a decrease in maximum force with decreasing pH. Together, these mechanisms can reproduce the experimentally observed steady-state pH-dependent force-Ca curves (Fig. 2D). This is consistent with the study by Crampin and Smith (9) who also used two distinct mechanisms to capture the pH-dependent force-Ca data, but by using a phenomenological model for force generation. Our model also suggests that only one H^+ binds to the Ca^{2+} binding site and that the release of the metabolic H^+ occurs during the power-stroke and after the release of Pi.

Model limitations

This model of Ca^{2+} activation and cross-bridge kinetics is a mean-field representation of cooperative spatial interactions between regulatory proteins and cross-bridge action. Rather than explicitly describing these spatial interactions, which would require computationally-intensive PDEs, the model achieves this by using a mean value to represent the population as a whole and, in doing so, can be described using a set of ODEs. The gains, in terms of computational efficiency, of this approach are offset by the limitations imposed on modeling the feedback behaviour. Rice et al. (42) have shown that mean-field models generate hysteresis artifacts not seen in real muscle when global feedback on Ca^{2+}-binding affinity is incorporated *i.e.,* allowing strongly-bound cross-bridges to influence explicitly the affinity of Ca^{2+} binding. But feedback mechanisms onto the Ca^{2+} affinity for troponin C are necessary for simulating observed phenomena such as ADP-contraction (33, 43, 44) and spontaneous oscillatory contractions (45, 46). These phenomena have been successfully simulated using models with different feedback mechanisms, although it must be pointed out that these models are designed to study these specific phenomena only and cannot simulate other behaviour such as force-Ca relations (33, 46).

Inversion of the force-MgADP relationship

One of the unexpected outcomes from this modeling study is the dependence of the force-MgADP relationship on the other metabolites: MgATP, Pi and H^+. Fig. 3A shows a reversal point at [MgATP] = 0.9 mM where the MgADP-dependent curves intersect. At this point, isometric force is *insensitive* to the MgADP concentration. For [MgATP] < 0.9 mM, an increase in MgADP concentration leads to a decrease in force, whereas for [MgATP] > 0.9 mM, increasing MgADP increases force. Varying [MgADP] and [Pi] will shift the position of this reversal point. This effect is limited not just to MgATP as the trend of the force-MgADP curve also depends on $[H^+]$ and all the other parameters in the cross-bridge cycle. This reversal behaviour is unique to the MgADP binding step as the sensitivity of force to [MgATP], [Pi] and $[H^+]$ will exhibit only a unidirectional response. This emergent feature of the model appears consistent with data showing a biphasic force-MgADP curve that initially increases with increasing MgADP before inverting and decreasing as MgADP is further increased (figure 5 from Shimizu et al. (43)). Our model is able to reproduce qualitatively this biphasic behaviour if we assume that [Pi] is increasing commensurate with [MgADP] (see Fig. S3 of Supporting Material). The increasing [Pi] tilts the balance of XB_{PostR} towards $AM2$ such that further increases in [MgADP] will increase the fraction of cross-bridges in state XB_{PreR} which is a non-force-generating state under isometric conditions. The mechanism underlying this behaviour is centered around the placement of the MgADP binding step between the two strongly-bound sub-states that make up XB_{PostR} ($AM1$ and $AM2$). The direction of the force-MgADP relationship depends on the balance between the competition for these two states. An analysis of this reversal point and the conditions under which it occurs is provided in the Supporting Material.

Reversibility

In our model of the cross-bridge cycle, the value of f_{xbT} is calculated to be minute. The small magnitude of this reverse rate constant restricts the cross-bridge from cycling backwards to any appreciable extent. Despite this, it is obligatory to include f_{xbT} to ensure that the cycle is thermodynamically consistent. Simulation of muscle stretch under conditions where the free energy was artificially set to be positive produced a very small reversal flux. This is consistent with many studies in the literature that have attempted, but failed, to generate ATP through the application of external work (47–

50). Our model shows that the cross-bridge cycle can reverse, albeit at a very low rate, and this is primarily due to the kinetics of the cross-bridge cycle.

Implications for ischemia

Our simulation of ischemia shows an exponential-like decrease in force which falls to approximately 10% after 10 minutes of ischemia (Fig. 5). These results are consistent with the experimental data of Befroy et al. (38) from perfused guinea pig hearts. We have isolated the effects of the metabolic changes on the cross-bridge cycle from effects of changing Ca^{2+} levels by setting a high $[Ca^{2+}]$. By considering each of the metabolite time-courses separately, the sensitivity analysis suggests that [Pi] and pH are the primary contributors to the rapid fall in maximum tension during ischemia (Fig. 5). However, the metabolic changes that occur during ischemia also have direct effects on SERCA and the Na-pump, while falling pH directly inhibits the ryanodine receptors and indirectly leads to a rise in intracellular $[Na^{+}]$ (see (9) and references therein). Inhibition of SERCA and elevation of intracellular $[Na^{+}]$ will contribute to a rise in the diastolic Ca^{2+} concentration and the amplitude of the Ca^{2+} transient while the force production decreases. Row E of Fig. 5 shows that an increase in $[Ca^{2+}]$ cannot restore the loss of contractile strength brought about by the rise in [Pi] and fall in pH. Furthermore the fall in pH greatly reduces the sensitivity of the force-Ca response, pushing the Ca_{50} past 10 μM after 10 minutes of ischemia.

The model developed here incorporates metabolite dependence into a model of cooperative activation and cross-bridge kinetics, that can reproduce a range of important metabolite/force/length/Ca^{2+} characteristics. The model is constructed using ordinary differential equations, making it ideal for integrating into whole-cell models of excitation-contraction. The simulations of ischemia in this study were carried out by imposing the time-course of metabolic changes onto our model. The next step is to integrate this cross-bridge model into a cellular framework and to couple it to a model of mitochondrial oxidative phosphorylation, such that the metabolic time-courses are driven by the mitochondria which, in turn, drive the cross-bridge model. Along with published models of the cardiac Na-pump (2, 10) and SERCA (11), this metabolite-sensitive model of the cross-bridge cycle provides a platform on which to developing a whole-cell model of cardiac electrophysiology and Ca^{2+} dynamics that is capable of simulating the effects of compromised energetics during ischemia.

The model is available in the CellML repository at 'models.cellml.org'. Full details and further analysis of the model is available in the Supporting Materials.

This work was supported by a Tertiary Education Commission (New Zealand) Top Achiever Doctoral Scholarship to KT; Royal Society of New Zealand (Marsden Fund no. 06-UoA-123) to DSL and NPS; National Institute of Biomedical Imaging and Bioengineering grant no. EB-005825 to EJC and NPS; Engineering and Physical Sciences Research Council grant no. EP/G007521 to NPS.

This publication is based on work (EJC) supported in part by Award No KUK-C1-013-04, made by King Abdullah University of Science and Technology (KAUST).

APPENDIX

All parameters in the Extended Model are as given in (8) except $xbmod_{species} = 0.2$ as described above. Three new parameters are introduced: $k_{dHCa} = 2 \times 10^{-5}$ mM, $m = 1$ and $k_{dADP} = 4$ μM.

The following ordinary differential equations describing the cross-bridge kinetics are modified from Eqs. 14-17 from (8):

$$\begin{aligned}
\frac{d}{dt}P_{XB} &= k_{npT} \times N_{XB} - (k_{pnT} + \alpha_1^+) \times P_{XB} \\
\frac{d}{dt}XB_{PreR} &= \alpha_1^+ \times P_{XB} + \alpha_2^- \times XB_{PostR} - (\alpha_1^- + \alpha_2^+) \times XB_{PreR} \\
\frac{d}{dt}XB_{PostR} &= \alpha_3^- \times P_{XB} + \alpha_2^+ \times XB_{PreR} - (\alpha_2^- + \alpha_3^+) \times XB_{PostR} \\
N_{XB} &= 1 - (P_{XB} + XB_{PreR} + XB_{PostR})
\end{aligned}$$

where

$$\begin{aligned}
\alpha_1^+ &= f_{appT} \\
\alpha_2^+ &= h_{fT} \\
\alpha_1^- &= [\mathrm{Pi}] \times g'_{appT} \\
\alpha_3^- &= f_{xbT}
\end{aligned}$$

and α_2^-, α_3^+ are defined by Eqs 10 and 9 respectively. f_{appT}, h_{fT}, are rate constants from (8) and g'_{xbT}, g'_{appT} and h'_{bT} are defined in Eqs. 3, 5 and 7, respectively. f_{xbT} is calculated using the constraint Eq. 1:

$$f_{xbT} = \frac{k_{dADP} \times f_{appT} \times h_{fT} \times g'_{xbT}}{g'_{appT} \times h'_{bT} \times k_{MgATP}} \tag{11}$$

where $k_{MgATP} = 15400$ mM^2 is the equilibrium constant for the ATP hydrolysis reaction and is defined as $k_{MgATP} = e^{-\Delta G^0/RT}$. $\Delta G^0 = 10.3$KJ mol^{-1} is the standard free energy change taking into account [H$^+$] in the hydrolysis reaction (Eq. 2), R is the universal gas constant and $T = 298$ K.

The differential equations governing the rate of change of the mean distortions, Eqs. 29 and 30 of (8) are also modified:

$$\begin{aligned}
\frac{d}{dt}xXB_{PreR} &= \frac{1}{2}\frac{dSL}{dt} + \frac{\phi}{XB_{PreR}^{DutyFract}}\left[-(\alpha_1^+ \times xXB_{PreR})\right. \\
&\qquad \left. + \alpha_2^- \times (xXB_{PostR} - x_0 - xXB_{PreR})\right] \\
\frac{d}{dt}xXB_{PostR} &= \frac{1}{2}\frac{dSL}{dt} + \frac{\phi}{XB_{PostR}^{DutyFract}}\left[\alpha_2^+ \times (xXB_{PreR} + x_0 - xXB_{PostR})\right]
\end{aligned}$$

Addition of f_{xbT} modifies Eqs. 31 and 32 of (8), used to calculate the steady-state occupancies of XB_{PreR} and XB_{PostR}:

$$\begin{aligned}
XB_{PreR}^{DutyFract} &= \frac{\alpha_3^-\alpha_2^- + \alpha_3^+\alpha_1^+ + \alpha_2^-\alpha_1^+}{\Sigma_{XB}^{DutyFract}} \\
XB_{PostR}^{DutyFract} &= \frac{\alpha_1^+\alpha_2^+ + \alpha_3^-\alpha_1^- + \alpha_3^-\alpha_2^+}{\Sigma_{XB}^{DutyFract}} \\
\Sigma_{XB}^{DutyFract} &= \alpha_1^+\alpha_2^+ + \alpha_3^-\alpha_1^- + \alpha_3^-\alpha_2^+ + \alpha_3^-\alpha_2^- + \\
&\quad \alpha_3^+\alpha_1^+ + \alpha_2^-\alpha_1^+ + \alpha_2^+\alpha_3^+ + \alpha_3^-\alpha_1^- + \alpha_3^+\alpha_1^-
\end{aligned}$$

Equations 33 and 34 in (8), used to normalise the force output, become:

$$\begin{aligned}
XB_{PreR}^{Max} &= \frac{f_{xb}h_b + g_{xb}f_{app} + h_{bT}f_{app}}{\Sigma_{XB}^{Max}} \\
XB_{PostR}^{Max} &= \frac{f_{app}h_f + f_{xb}g_{app} + f_{xb}h_b}{\Sigma_{XB}^{Max}} \\
\Sigma_{XB}^{Max} &= h_f g_{xb} + h_b g_{app} + g_{xb}g_{app} + f_{xb}h_b + g_{xb}f_{app} + \\
&\quad h_b f_{app} + f_{xb}g_{app} + f_{app}h_f + f_{xb}h_b
\end{aligned}$$

In the Extended Model, the normalising force is therefore determined by the force at the reference physiological metabolite levels under "optimal conditions" (see (8) for details). f_{xb} is defined similarly to Eq.11, except that the base value of the rate constant is used *i.e.,* f_{app} instead of f_{appT}.

References

1. Allen, D. G., and C. H. Orchard, 1987. Myocardial contractile function during ischemia and hypoxia. *Circ Res* 60:153–168.

2. Smith, N. P., and E. J. Crampin, 2004. Development of models of active ion transport for whole-cell modelling: cardiac sodium-potassium pump as a case study. *Prog Biophys Mol Biol* 85:387–405.

3. Kawai, M., Y. Saeki, and Y. Zhao, 1993. Crossbridge scheme and the kinetic constants of elementary steps deduced from chemically skinned papillary and trabecular muscles of the ferret. *Circ Res* 73:35–50.

4. Hunter, P. J., A. D. McCulloch, and H. E. ter Keurs, 1998. Modelling the mechanical properties of cardiac muscle. *Prog Biophys Mol Biol* 69:289–331.

5. Hill, T. L., 1989. Free energy transduction and biochemical cycle kinetics. Springer-Verlag New York Inc.

6. Huxley, A. F., 1957. Muscle structure and theories of contraction. *Prog Biophys Mol Biol* 7:255.

7. Pate, E., and R. Cooke, 1989. A model of crossbridge action—the effects of ATP, ADP and Pi. *J Musc Res Cell Motil* 10:181–196.

8. Rice, J. J., F. Wang, D. M. Bers, and P. P. de Tombe, 2008. Approximate model of cooperative activation and crossbridge cycling in cardiac muscle using ordinary differential equations. *Biophys J* 95:2368–2390.

9. Crampin, E. J., and N. P. Smith, 2006. A dynamic model of excitation-contraction coupling during acidosis in cardiac ventricular myocytes. *Biophys J* 90:3074–3090.

10. Terkildsen, J. R., E. J. Crampin, and N. P. Smith, 2007. The balance between inactivation and activation of the Na^+–K^+ pump underlies the triphasic accumulation of extracellular K^+ during myocardial ischemia. *Am J Physiol* 293:H3036–H3045.

11. Tran, K., N. P. Smith, D. S. Loiselle, and E. J. Crampin, 2009. A thermodynamic model of the cardiac sarcoplasmic/endoplasmic Ca(2+) (SERCA) pump. *Biophys J* 96:2029–2042.

12. Palmer, S., and J. C. Kentish, 1998. Roles of Ca^{2+} and crossbridge kinetics in determining the maximum rates of Ca^{2+} activation and relaxation in rat and guinea pig skinned trabeculae. *Circ Res* 83:179–186.

13. Lymn, R. W., and E. W. Taylor, 1971. Mechanism of adenosine triphosphate hydrolysis by actomyosin. *Biochemistry* 10:4617–4623.

14. Goldman, Y. E., 1987. Kinetics of the actomyosin ATPase in muscle-fibers. *Annu Rev Physiol* 49:637–654.

15. Cooke, R., 1997. Actomyosin interaction in striated muscle. *Physiol Rev* 77:671–697.

16. Bers, D. M., 2001. Excitation-Contraction Coupling And Cardiac Contractile Force. Kluwer Academic Publishers, second edition.

17. Cooke, R., and E. Pate, 1985. The effects of ATP and phosphate on the contraction of muscle-fibers. *Biophys J* 48:789–798.

18. Ebus, J. P., Z. Papp, R. Zaremba, and G. J. M. Stienen, 2001. Effects of MgATP on ATP utilization and force under normal and simulated ischaemic conditions in rat cardiac trabeculae. *Pflügers Arch* 443:102–111.

19. Hibberd, M. G., J. A. Dantzig, D. R. Trentham, and Y. E. Goldman, 1985. Phosphate release and force generation in skeletal-muscle fibers. *Science* 228:1317–1319.

20. Dantzig, J. A., J. W. Lacktis, E. Homsher, and Y. E. Goldman, 1987. Mechanical transients initiated by photolysis of caged-Pi during active skeletal-muscle contractions. *Biophys J* 51:A3–A3.

21. Godt, R. E., and T. M. Nosek, 1989. Changes of intracellular milieu with fatigue or hypoxia depress contraction of skinned rabbit skeletal and cardiac-muscle. *J Physiol* 412:155–180.

22. Kentish, J. C., 1986. The effects of inorganic-phosphate and creatine-phosphate on force production in skinned muscles from rat ventricle. *J Physiol* 370:585–604.

23. Fabiato, A., and F. Fabiato, 1978. Effects of pH on myofilaments and sarcoplasmic-reticulum of skinned cells from cardiac and skeletal-muscles. *J Physiol* 276:233–255.

24. Orchard, C. H., and J. C. Kentish, 1990. Effects of changes of pH on the contractile function of cardiac-muscle. *Am J Physiol* 258:C967–C981.

25. Blanchard, E. M., and R. J. Solaro, 1984. Inhibition of the activation and troponin calcium-binding of dog cardiac myofibrils by acidic pH. *Circ Res* 55:382–391.

26. Solaro, R. J., S. C. Elsaleh, and J. C. Kentish, 1989. Ca^{2+}, pH and the regulation of cardiac myofilament force and ATPase activity. *Molec Cell Biochem* 89:163–167.

27. Rodger, C. D., and R. T. Tregear, 1974. Crossbridge angle when ADP is bound to myosin. *J Mol Biol* 86:495–497.

28. Schoenberg, M., and E. Eisenberg, 1987. ADP binding to myosin cross-bridges and its effect on the cross-bridge detachment rate constants. *J Gen Physiol* 89:905–920.

29. Xu, S., J. Gu, S. Frisbie, and L. C. Yu, 1998. Structural changes in rigor (nucleotide-free) cross-bridges induced by the addition of MgADP. *Biophys J* 74:A363–A363.

30. Dantzig, J. A., M. G. Hibberd, D. R. Trentham, and Y. E. Goldman, 1991. Cross-bridge kinetics in the presence of MgADP investigated by photolysis of caged ATP in rabbit psoas muscle-fibers. *J Physiol* 432:639–680.

31. Takezawa, Y., D. S. Kim, M. Ogino, Y. Sugimoto, T. Kobayashi, T. Arata, and K. Wakabayashi, 1999. Backward movements of cross-bridges by application of stretch and by binding of MgADP to skeletal muscle fibers in the rigor state as steadied by X-ray diffraction. *Biophys J* 76:1770–1783.

32. Karatzaferi, C., K. H. Myburgh, M. K. Chinn, K. Franks-Skiba, and R. Cooke, 2003. Effect of an ADP analog on isometric force and ATPase activity of active muscle fibers. *Am J Physiol Cell Physiol* 284:C816–C825.

33. Fukuda, N., H. Fujita, T. Fujita, and S. Ishiwata, 1998. Regulatory roles of MgADP and calcium in tension development of skinned cardiac muscle. *J Muscle Res Cell Motil* 19:909–921.

34. Kentish, J. C., 1991. Combined inhibitory actions of acidosis and phosphate on maximum force production in rat skinned cardiac-muscle. *Pflügers Arch* 419:310–318.

35. Mekhfi, H., and R. Ventura-Clapier, 1988. Dependence upon high-energy phosphates of the effects of inorganic-phosphate on contractile properties in chemically skinned rat cardiac fibers. *Pflügers Arch* 411:378–385.

36. Johnson, R. E., and P. H. Adams, 1984. ADP binds similarly to rigor muscle myofibrils and to actomyosin-subfragment one. *FEBS Letters* 174:11–14.

37. Kardami, E., S. D. Bruin, and W. Gratzer, 1979. Interaction of ADP with skeletal and cardiac myosin and their active fragments observed by proton release. *Eur J Biochem* 97:547–552.

38. Befroy, D. E., T. Powell, G. K. Radda, and K. Clarke, 1999. Osmotic shock: modulation of contractile function, pH(i), and ischemic damage in perfused guinea pig heart. *Am J Physiol* 276:H1236–H1244.

39. Campbell, K. B., M. V. Razumova, R. D. Kirkpatrick, and B. K. Slinker, 2001. Nonlinear myofilament regulatory processes affect frequency-dependent muscle fiber stiffness. *Biophys J* 81:2278–2296.

40. Razumova, M. V., A. E. Bukatina, and K. B. Campbell, 1999. Stiffness-distortion sarcomere model for muscle simulation. *J Appl Physiol* 87:1861–1876.

41. Solaro, R. J., J. A. Lee, J. C. Kentish, and D. G. Allen, 1988. Effects of acidosis on ventricular muscle from adult and neonatal rats. *Circ Res* 63:779–787.

42. Rice, J. J., Y. Tu, C. Poggesi, and P. P. De Tombe, 2008. Spatially-compressed cardiac myofilament models generate hysteresis that is not found in real muscle. *Pac Symp Biocomput* 366–77.

43. Shimizu, H., T. Fujita, and S. Ishiwata, 1992. Regulation of tension development by MgADP and Pi without Ca(2+) – role in spontaneous tension oscillation of skeletal-muscle. *Biophys J* 61:1087–1098.

44. Fukuda, N., H. Kajiwara, S. Ishiwata, and S. Kurihara, 2000. Effects of MgADP on length dependence of tension generation in skinned rat cardiac muscle. *Circ Res* 86:E1–E6.

45. Fukuda, N., H. Fujita, T. Fujita, and S. Ishiwata, 1996. Spontaneous tension oscillation in skinned bovine cardiac muscle. *Pflügers Arch* 433:1–8.

46. Smith, D. A., and D. G. Stephenson, 2009. The mechanism of spontaneous oscillatory contractions in skeletal muscle. *Biophys J* 96:3682–3691.

47. Curtin, N. A., and R. E. Davies, 1973. Chemical and mechanical changes during stretching of activated frog skeletal-muscle. *Cold Spring Harbor Symposia On Quantitative Biology* 37:619–626.

48. Infante, A. A., D. Klaupiks, and R. E. Davies, 1964. Adenosine Triphosphate: Changes in muscles doing negative work. *Science* 144:1577–1578.

49. Curtin, N. A., D. D. Drobnis, R. E. Larson, and R. E. Davies, 1969. Very low ATP usage with very high tension in activated muscles during a slow stretch. *Federation Proceedings* 28:711.

50. Linari, M., R. C. Woledge, and N. A. Curtin, 2003. Energy storage during stretch of active single fibres from frog skeletal muscle. *J Physiol* 548:461–474.

Figure 1

(***A***) Original model from Rice et al. 2008. (***B***) The original model is modified to include metabolite dependence (Extended Model). The dotted ellipse indicates the two strongly-bound rapid-equilibrium states. The rate constants g'_{appT}, g'_{xbT} and h'_{bT} are true first order rate constants that are independent of metabolite concentrations whereas g_{appT}, g_{xbT} and h_{bT} from the original model are pseudo-first order rate constants which are assumed to be implicit functions of MgATP, MgADP, Pi and H^+. (See text for details) (***C***) Schematic of the competitive binding of H^+ to the Ca^{2+} binding site on troponin C. The dotted rectangle indicates the two states that are assumed to be in rapid equilibrium. The on-rate for Ca^{2+} binding, k'_{onT}, is modified to include the H^+ regulation.

Figure 2

(***A***) Comparing the effect of modeling the Pi binding step at either g_{appT} or h_{bT} on the force-Pi curve. The data points are from rabbit papillary muscle (Godt and Nosek, 1989). Other conditions in the simulations: [MgATP] = 5 mM, [MgADP] = 36.3 μM, pH = 7.15, $[Ca^{2+}]_i$ = 200 uM (maximum activation), SL = 2.2 μm, T = 22 °C. (***B***) Best fit of the relative Ca^{2+} sensitivities (Ca_{50}) of the Extended Model to data from Orchard and Kentish, 1990, at $m = 1$ ($k_{dHCa} = 2 \times 10^{-5}$ mM) and at $m = 2$ ($k_{dHCa} = 1.8 \times 10^{-4}$ mM^2). The Ca_{50} values on the y axis are normalised to the Ca_{50} at pH = 7. (***C***) Model simulation of maximum steady-state force (under saturated Ca^{2+} conditions) as a function of pH. The model simulations correspond to the placement of the metabolic H^+ release step at either g_{appT} or h_{bT} in the cross-bridge cycle. The simulations are normalised to force at pH 7.2 (see Supporting Materials for original data). (***D***) Model simulation of steady-state force-Ca curves as a function of pH. Other conditions in the simulations of ***B***, ***C*** and ***D***: SL = 2.1 μM, T = 30 °C and metabolite concentrations are set to their reference values.

Figure 3

(***A***) Model simulations of isometric force as a function of MgATP concentration at different MgADP concentrations. The data points are from rat ventricular tissue (Ebus et. al., 2001) for which MgADP concentration is not specified and therefore assumed to be low / zero. The simulated curves are normalised to the maximum force from the data. Other conditions in the simulation: [Pi] = 0 mM, pH = 7, $[Ca^{2+}]$ = 200 μM, SL = 2.1 μM and T =

20 °C. (***B***) Model simulations of the time course of isometric force recovery after a sudden length change as a function of MgATP concentration. The change in length is applied at 300 ms (see text for details). The curves are normalised to the maximum force at [MgATP] = 0.1 mM. Other conditions are [MgADP] = 1 μM, [Pi] = 2 mM, pH = 7, [Ca^{2+}] = 200 μM, SL = 2.1 μM and T = 20 °C. (***C***) Same simulation as ***B*** except that each curve has been normalised to its own maximum force so that the rate of force redevelopment at different MgATP concentrations can be compared to data shown in: (***D***) Experimental data reproduced from Fig. 5A of Ebus et al. (2001).

Figure 4

Two measures of complex stiffness: dynamic modulus (***A***) and phase shift (***B***), calculated for the model as a function of perturbation frequency and [Pi]. ***C*** and ***D*** show experimental data from ferret cardiac muscle (reproduced from Figs. 4A and 4B from Kawai et al. 1993) (permission requested). Dynamic modulus is calculated as the amplitude of the normalised force oscillation in response to a sinusoidal length change protocol with an amplitude of 0.25% L_0 (where L_0 is set at 2.28 μm). Other conditions in the simulations: [MgATP] = 5 mM, pH = 7.15, [Ca^{2+}] = 200 μM and T = 20 °C. We also assume [MgADP] = 0 as there was no mention of its presence in the experimental protocol described by Kawai et al.

Figure 5

Production of force during ischemia. Imposed ischemic time-courses for metabolites and pH, and simulated force are shown in the first column. The time-courses for the change in [MgATP] (***A***), [Pi] (***B***), [MgADP] (***C***) and pH (***D***) are redrawn at five distinct time points (T = 0, 2.5, 5, 10 and 15 min) from Befroy et al. (1999) and Terkildsen et al. (2007). These time courses are then used to simulate the isometric force response (row ***E***). The other four columns show the sensitivity of maximal force to [MgATP], [Pi], [MgADP] pH and [Ca^{2+}] at four different time points during ischemia. The Y-axis of each plot shows normalised force. Each column illustrates a particular time point after the onset of ischemia. Filled circles indicate the force and respective metabolite, pH or Ca^{2+} level at that time point. Curves represent the effect on force (sensitivity) of changing one of: [MgATP], [Pi], [MgADP], pH or [Ca^{2+}] (rows ***A*** to ***E***), while keeping the others constant. For plots ***A*** to ***D***, [Ca^{2+}] is held at 200 μM so as to achieve maximum force. Other conditions in the simulations: SL = 2.2 μM and T = 25 °C.

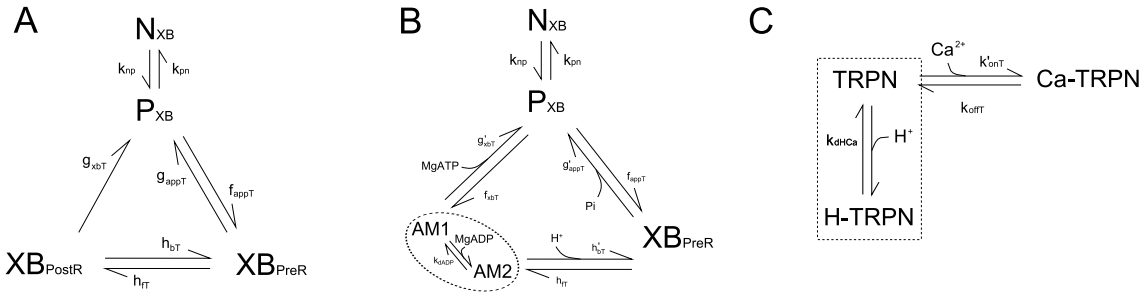
A
N_XB
k_np
k_pn
P_XB
g_xbT
g_appT
f_appT
h_bT
XB_PostR
XB_PreR
h_fT
B
N_XB
k_np
k_pn
P_XB
g'_xbT
MgATP
f_xbT
g'_appT
f_appT
Pi
AM1
MgADP
k_dADP
AM2
H+
h'_bT
XB_PreR
h_fT
C
Ca2+
k'_onT
TRPN
Ca-TRPN
k_offT
k_dHCa
H+
H-TRPN

Figure 1:

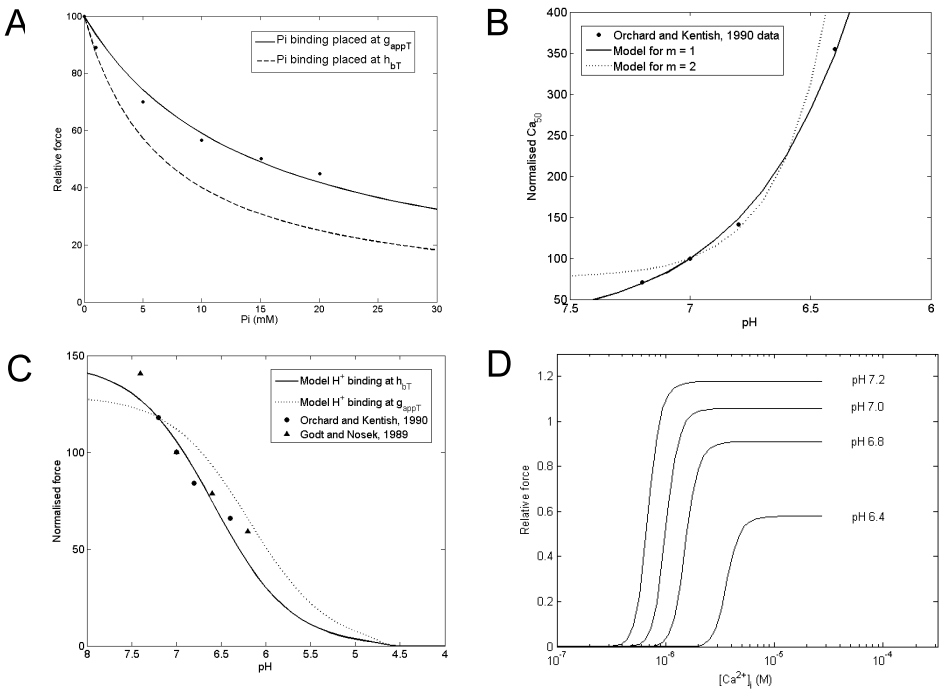
A
Pi binding placed at g_{appT}
Pi binding placed at h_{bT}
Relative force
Pi (mM)
B
Orchard and Kentish, 1990 data
Model for m = 1
Model for m = 2
Normalised Ca_{50}
pH
C
Model H^+ binding at h_{bT}
Model H^+ binding at g_{appT}
Orchard and Kentish, 1990
Godt and Nosek, 1989
Normalised force
pH
D
pH 7.2
pH 7.0
pH 6.8
pH 6.4
Relative force
$[Ca^{2+}]_i$ (M)

Figure 2:

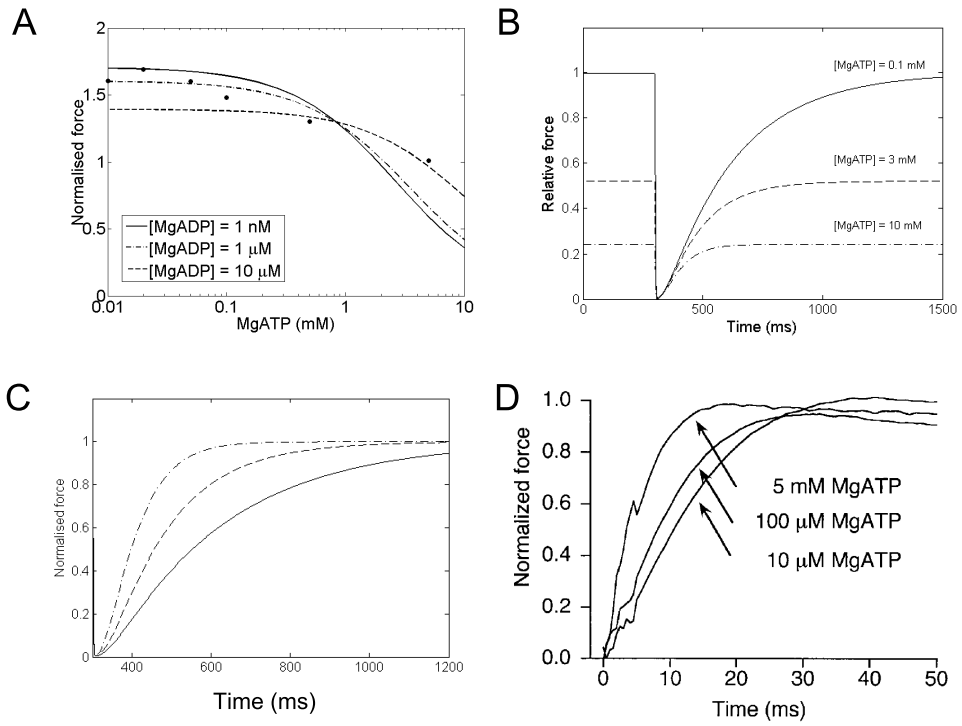
A
Normalised force
MgATP (mM)
[MgADP] = 1 nM
[MgADP] = 1 μM
[MgADP] = 10 μM
B
Relative force
Time (ms)
[MgATP] = 0.1 mM
[MgATP] = 3 mM
[MgATP] = 10 mM
C
Normalised force
Time (ms)
D
Normalized force
Time (ms)
5 mM MgATP
100 μM MgATP
10 μM MgATP

Figure 3:

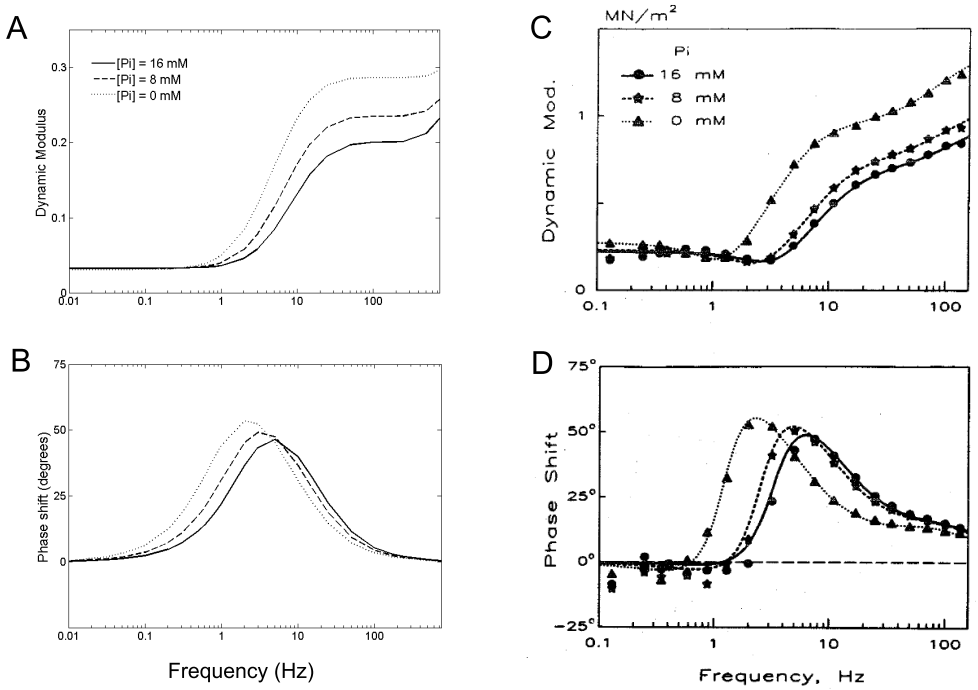
A
[Pi] = 16 mM
[Pi] = 8 mM
[Pi] = 0 mM
Dynamic Modulus
0.3
0.2
0.1
0
0.01
0.1
1
10
100
B
Phase shift (degrees)
75
50
25
0
0.01
0.1
1
10
100
Frequency (Hz)
C
MN/m²
Pi
16 mM
8 mM
0 mM
Dynamic Mod.
1
0
0.1
1
10
100
D
75°
50°
25°
0°
-25°
Phase Shift
0.1
1
10
100
Frequency, Hz

Figure 4:

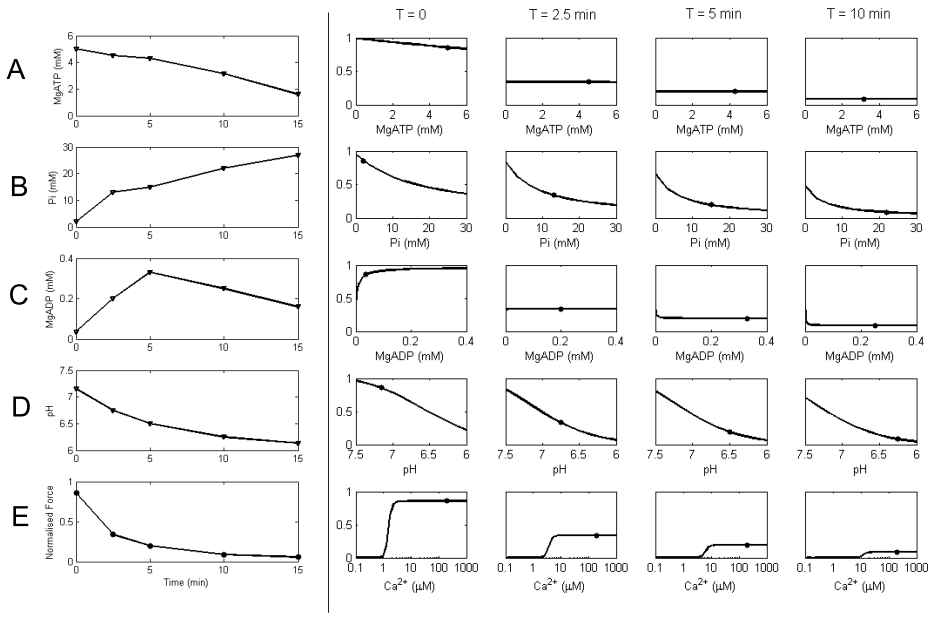
A
B
C
D
E
MgATP (mM)
Pi (mM)
MgADP (mM)
pH
Normalised Force
Time (min)
T = 0
T = 2.5 min
T = 5 min
T = 10 min
MgATP (mM)
Pi (mM)
MgADP (mM)
pH
Ca2+ (μM)

Figure 5:

RECENT REPORTS

09/09	Equilibrium Order Parameters of Liquid Crystals in the Laudau-De Gennes Theory	Majumdar
10/09	Landau-De Gennes theory of nematic liquid crystals: the Oseen-Frank limit and beyond	Majumdar Zarnescu
11/09	A Comparison of Numerical Methods used for Finite Element Modelling of Soft Tissue Deformation	Pathmanathan Gavaghan Whiteley
12/09	From Individual to Collective Behaviour of Unicellular Organisms: Recent Results and Open Problems	Xue Othmer Erban
13/09	Stochastic modelling of reaction-diffusion processes: algorithms for bimolecular reactions	Erban Chapman
14/09	Chaste: a test-driven approach to software development for physiological modelling	Pitt-Francis *et al.*
15/09	Block triangular preconditioners for PDE constrained optimization	Rees Stoll
16/09	From microscopic to macroscopic descriptions of cell migration on growing domains	Baker Yates Erban
17/09	The Influence of Gene Expression Time Delays on Gierer-Meinhardt Pattern Formation Systems	Seirin Lee Gaffney Monk
18/09	Analysis of a stochastic chemical system close to a sniper bifurcation of its mean field model	Erban *et al.*
19/09	On the existence and the applications of modified equations for stochastic differential equations	Zygalakis
20/09	Pebble bed: reflector treatment and pressure velocity coupling	Charpin *et al.*
21/09	A finite difference method for free boundary problems	Fornberg
22/09	Tangent unit-vector fields: nonabelian homotopy invariants and the Dirichlet energy	Majumdar Robbins Zyskin
23/09	Morphological instability of a nonequilibrium icecolloid interface	Peppin Majumdar Wettlaufer

24/09	The effect of polar lipids on tear film dynamics	Aydemir Breward Witelski
25/09	Preconditioning for active set and projected gradient methods as semi-smooth Newton methods for PDE-constrained optimization with control constraints	Stoll Wathen
26/09	Functional differential equations arising in cell-growth	Wake Begg
27/09	A Cell Growth Model Revisited	Derfel van Brunt Wake
28/09	Quasi-steady state reduction of molecular motor-based models of directed intermittent search	Newby Bressloff
29/09	All-at-once preconditioning in PDE-constrained optimization	Rees Stoll Wathen
30/09	An hp-Local Discontinuous Galerkin method for Parabolic Integro-Differential Equations	Pani Yadav
31/09	Stochastic neural field theory and the system-size expansion	Bressloff
32/09	A Hamiltonian Krylov-Schur-type method based on the symplectic Lanczos process	Benner Faßbender Stoll
33/09	Nematic liquid crystals : from Maier-Saupe to a continuum theory	Ball Majumdar
34/09	Tangent unit-vector fields: nonabelian homotopy invariants and the Dirichlet energy	Majumdar Robbins Zyskin

Copies of these, and any other OCCAM reports can be obtained from:

Oxford Centre for Collaborative Applied Mathematics
Mathematical Institute
24 - 29 St Giles'
Oxford
OX1 3LB
England
www.maths.ox.ac.uk/occam